

# FEDSM2021-65621

## **SOLUTION-RESPONSIVE PARTICLE SIZE ADAPTIVITY IN LAGRANGIAN VORTEX PARTICLE METHODS**

**Mark J. Stock**

Applied Scientific Research, Inc.  
Irvine, California  
Email: markjstock@gmail.com

**Adrin Gharakhani**

Applied Scientific Research, Inc.  
Irvine, California  
adrin@applied-scientific.com

### **ABSTRACT**

*In order to minimize the computational resources necessary for a given level of accuracy in a Lagrangian Vortex Particle Method, a novel particle core size adaptivity scheme has been created. The method adapts locally to the solution while preventing large particle size gradients, and optionally adapts globally to focus effort on important regions. It is implemented in the diffusion solver, which uses the Vorticity Redistribution Method, by allowing and accounting for variations in the core radius of participating particles. We demonstrate the effectiveness of this new method on the diffusion of a  $\delta$ -function and impulsively started flow over a circular cylinder at  $Re = 9,500$ . In each case, the adaptive method provides solutions with marginal loss of accuracy but with substantially fewer computational elements.*

### **NOMENCLATURE**

$C_2$	2nd moment of a distribution along the x- or y-axis.
$D$	Diameter.
$h$	Cell size.
$h_\nu$	Diffusion length scale.
$N_\nu$	Number of vortex particles.
$R$	Radius.
$Re$	Reynolds number.
$t$	Time.
$t_R$	Time non-dimensionalized by radius.
$\mathbf{u}$	Velocity vector.
$\mathbf{U}_\infty$	Freestream velocity vector.
$\mathbf{x}$	Position vector.

$\Gamma$  Circulation ( $\omega dA$  in 2-D).

$\Delta t$  Computational time step.

$\Delta x$  Cell size or interparticle spacing.

$\varepsilon$  Strength threshold, relative or absolute.

$\nu$  Kinematic viscosity.

$\sigma$  Core radius of particle smoothing function.

$\omega$  Vorticity.

### **INTRODUCTION**

Lagrangian Vortex Particle Methods (LVPM) are regularly used to simulate highly-unsteady vortical flows, often with many moving boundaries, and at high Reynolds numbers. As a continuous vorticity field must be represented by a finite number of particles, and computational expense scales at best linearly with the number of particles, methods to control the number of computational elements are necessary for practical simulations.

Early LVPM implementations either disregarded diffusion altogether, or treated it with random walk [1] or core-spreading [2] methods, each of which did not require generation of new particles. When Greengard [3] showed that core-spreading was not convergent due to lack of deformation of large particles, Rossi [4] resolved it by splitting large vortex blobs into many smaller ones. Since then, more accurate and convergent methods to account for diffusion emerged: the Particle Strength Exchange (PSE) [5, 6] and Vorticity Redistribution Methods (VRM) [7], both with the requirement that new particles be created at the outer reaches of the vorticity support to accommodate accurate diffusion.

The most basic methods for reducing  $N_v$  involve shrinking the vorticity-containing region. This is trivially accomplished by removing any vortex particles that pass through a plane or move far enough away from the study area to be considered irrelevant. An issue that emerges is that the absence of vorticity on the other side of this threshold makes the remaining vorticity “bounce” off the interface. Our experience shows that this can be suppressed by slowly weakening the particles as they pass through the threshold before removing them. The detrimental effects of modifying the vorticity can be controlled by simply moving this threshold farther downstream.

Most current methods to reduce particle count involve reducing the number of particles necessary to represent a given parcel of fluid; these involve merging, remeshing, and higher-order particles. Each of these methods is also able to accommodate the solution by varying the resolution or particle density.

Through the action of convection particle distributions become uneven and crowded. Merging (also called “lumping” or “fusion”) aims to reduce the crowding by identifying pairs or groups of nearby particles whose merging would least modify the vorticity. Spalart [8] discusses using a combination of size and strength as the merging criterion, and even suggests that it could be made more aggressive far from regions of interest, such as a far wake. Rossi [4] elaborates with a discussion of the error involved in merging, and provides formulas for minimizing errors in the first three moments. The author mentions the use of  $r ||\nabla \mathbf{u}||$  as a metric for spatial adaptivity, but does not demonstrate it. Dehnen [9], referring to astrophysical N-body simulations, proposes to use the threshold for merging to enforce pre-defined spatial adaptivity, allowing more aggressive merging in areas with lower spatial gradients. More recently, Lakkis & Ghoniem [10] conclude that merging of close particles can reduce particle count with a minimal effect on accuracy.

Remeshing is designed to reduce the errors due to scattered particle interpolation by generating new particles on a temporary regular mesh to replace a previous set of scattered particles [11, 12]. An advantage of this method is that its regularity allows the use of finite-difference methods to calculate diffusion. The grid used for remeshing does not have to be uniform and regular, but may use smoothly spatially-varying cell sizes, especially in the far wake [13–15], and thus the remeshing step generates larger particles in regions where the decrease in accuracy is deemed allowable. But this requires a remapping of the distorted grid to a uniform grid, which is typically predefined, and only globally solution-adaptive.

Barba *et al.* [16] demonstrate remeshing using Radial Basis Functions (RBFs) to be more accurate than regular-grid remeshing, and effective on irregular particle distributions. RBFs can theoretically remesh to any particle distribution, including one with more target points in areas with higher gradients. Reboux *et al.* [17] define methods for creating such a solution-adaptive particle distribution, and rely on an RBF or similar method to

initialize a new set of particles from an old set.

Of course, remeshing may also be done with an adaptive-mesh-refined (AMR) grid, which supports dynamic regions with incremental-resolution (usually  $2\times$ ) grids. Bergdorf *et al.* [18] apply these methods to refine cells, but use only the lowest resolution data to advance the solution. In addition, the method imposes a CFL-like condition on the time step to accommodate the algorithmic growth of the domain at any given resolution. Rasmussen *et al.* [19] present a hybrid Lagrangian-Eulerian Vortex-In-Cell (VIC) method using an AMR grid instead of the traditional grid. In VIC, a temporary grid is used only to accelerate calculation of the velocity field, not to remesh particles. In this work, a small number of large regions of the flow are tagged for refinement, though regular grid calculations can proceed with greater efficiency than scattered particle methods.

Finally, if particles are allowed to deform due to convection, forming ovals or higher-order shapes, fewer particles should be necessary to represent any given vorticity field, though other portions of the LVPM, such as the Biot-Savart integration become more difficult [20–23].

Relatively little work to date has demonstrated true, solution-responsive particle size adaptivity. While the AMR regridding of Bergdorf *et al.* [18] and the hybrid VIC work of Rasmussen *et al.* [19] were successful, the zones of adaptivity were large and strongly quantized (factors of 2 only). Lakkis & Ghoniem [10] present a method most similar to ours, in that particles perform core-spreading and/or VRM in order to achieve a desired particle core size. It does not, though, provide for solution-responsive adaptivity of particle core sizes, instead pre-defining the core size as a function of location. In order to minimize error, core sizes are quantized to  $\sigma^2 = 4m v \Delta t$  where  $m$  is an integer.

We propose a local (in time and space) and solution-adaptive method for determining and maintaining particle sizes for the solution of incompressible advection-diffusion problems. This is accomplished with a combination of VRM, core-spreading, and merging. Each particle’s strength (circulation in 2-D) serves as the criterion for adaptivity, and a particle radius-gradient limiter provides error control. The primary computational costs in the present method are the Biot-Savart integrations (which are trivial to parallelize) and the least-squares solutions to the VRM equations. As a result of these new methods, we have been able to achieve significant improvements in speed or accuracy for several canonical flow cases.

## PROPOSED METHOD

The software uses a desingularized LVPM to discretize the vorticity and an augmented Boundary Element Method (BEM) to enforce boundary conditions. These methods are summarized below, but extensive background [8, 24] and implementation-specific details [25–27] can be found elsewhere.

## Lagrangian Vortex Particle Methods

The governing equations of incompressible fluid flow in terms of the transport of vorticity are

$$\frac{\partial \boldsymbol{\omega}}{\partial t} + \boldsymbol{u} \cdot \nabla \boldsymbol{\omega} = \boldsymbol{\omega} \cdot \nabla \boldsymbol{u} + \frac{1}{\text{Re}} \nabla^2 \boldsymbol{\omega} \quad (1)$$

$$\nabla \cdot \boldsymbol{u} = 0 \quad (2)$$

$$\nabla \times \boldsymbol{u} = \boldsymbol{\omega} \quad (3)$$

supplemented with the appropriate velocity and vorticity boundary conditions. In two dimensions, vorticity is a scalar and the stretching term is identically zero. Specific details of the methods and algorithms used presently appear in our previous work [27].

In the LVPM, the vorticity field is discretized using  $N_v$  smooth vortex particles, assigned circulations  $\Gamma$ , and smooth core radius  $\sigma$ . Viscous diffusion is evaluated using the Vorticity Redistribution Method (see below). Velocities are computed from the integration of the Biot-Savart equation over the entire vorticity-containing region. A Boundary Element Method serves to enforce boundary condition at walls, and explicitly generates vorticity on the fluid side of the boundary. Convection is integrated using a second-order Runge-Kutta method. The convection and diffusion functions operate within a 2nd order operator-splitting scheme, in which one half step of diffusion is followed by a full convection step and then another half step of diffusion.

## Vorticity Redistribution Method

The Vorticity Redistribution Method (VRM) [7,28] is a powerful tool for calculating diffusion in a disordered collection of particles because it satisfies moment conservation up to arbitrary levels and automatically generates new particles where they are needed. In its original form, every particle has uniform core function and radius, simplifying the moment conservation equations that must be solved for the coefficients of strength exchange. They do not depend on the core radius or core function (shape) at all. This idea was later generalized to increase the accuracy of the popular Particle-Strength Exchange (PSE) for calculating diffusion among scattered particles [29].

In this and subsequent equations, we will consider only the two-dimensional case, but the extension to three dimensions is trivial. For a given particle at  $(x_i, y_i)$ , all nearby particles' positions  $(x_j, y_j)$  are transformed into a local frame around particle  $i$

and scaled by the diffusion length scale  $h_\nu$ .

$$\tilde{x}_j = \frac{x_j - x_i}{h_\nu} \quad (4)$$

$$\tilde{y}_j = \frac{y_j - y_i}{h_\nu} \quad (5)$$

$$h_\nu = \sqrt{\frac{\Delta t}{\text{Re}}} \quad (6)$$

The following set of equations for the 0th to 2nd moments of the distribution is then solved for the unknown fractions  $f_j$  of circulation that will be moved from particle  $i$  to particles  $j$ .

$$\sum_j f_j = 1 \quad (7)$$

$$\sum_j \tilde{x}_j f_j = 0 \quad (8)$$

$$\sum_j \tilde{y}_j f_j = 0 \quad (9)$$

$$\sum_j \tilde{x}_j^2 f_j = 2 \quad (10)$$

$$\sum_j \tilde{x}_j \tilde{y}_j f_j = 0 \quad (11)$$

$$\sum_j \tilde{y}_j^2 f_j = 2 \quad (12)$$

If a solution does not exist, a new particle is placed in the vicinity of particle  $i$ , at a specific distance  $\delta_\nu$ , and in the largest "hole" in the particle distribution, and the procedure is repeated.

The desired nominal separation between particles (used to insert new particles in the above procedure) and the particles' core radii are related to the diffusion length scale according to the following relationships.

$$\delta_\nu = C_\delta h_\nu \quad \text{particle nominal separation} \quad (13)$$

$$\sigma = C_\sigma \delta_\nu \quad \text{particle core radius} \quad (14)$$

These constants can vary somewhat and VRM will still provide a solution, with the constraint  $C_\delta \geq \sqrt{4}$ . The two-dimensional simulations below will use  $C_\delta = \sqrt{6}$  and  $C_\sigma = 2.0$ .

Additionally, a threshold circulation ( $\varepsilon$ ) is typically defined, below which a particle will not diffuse its strength to neighboring particles. This serves to limit the endless growth of particles on the fringes of the vorticity support. This threshold can be set to an absolute value, or as a fraction of the circulation of the strongest particle(s).

The above equations can be solved with the NNLS (non-negative least squares) solver available in Eigen [30]. This solver

will only distribute circulation to a number of neighbors equal to the total number of moment equations (6 for 2nd moments in 2-D). Alternatively, these VRM equations can be solved with a modified simplex solver [28, 31], which will distribute circulations to potentially all participating particles. The performance difference between these solvers is minimal.

### Extension to Variable-Radius Particles

For uniform-radius particles, the VRM equations are written as if each particle is a singular distribution (the moments of the core function of each particle cancel). To allow solution of the equations for particles with differing core radii, the moment conservation equations must be modified to account for the moments of vorticity of the particles' own cores. This modification to the original VRM equations was introduced by Lakkis & Ghoniem [32] in the context of axisymmetric diffusion. If we define  $\sigma_i$  to be the radius of particle  $i$  at the beginning of the diffusion step, and  $\tilde{\sigma}_i$  its radius at the end of the step, we must then solve the following set of equations for the unknown fractions  $f_j$  of circulation that will be moved from particle  $i$  to particles  $j$ .

$$\sum_j f_j = 1 \quad (15)$$

$$\sum_j \tilde{x}_j f_j = 0 \quad (16)$$

$$\sum_j \tilde{y}_j f_j = 0 \quad (17)$$

$$\sum_j \left( \tilde{x}_j^2 + C_2 \left( \frac{\tilde{\sigma}_j}{h_\nu} \right)^2 \right) f_j = 2 + C_2 \left( \frac{\sigma_i}{h_\nu} \right)^2 \quad (18)$$

$$\sum_j \tilde{x}_j \tilde{y}_j f_j = 0 \quad (19)$$

$$\sum_j \left( \tilde{y}_j^2 + C_2 \left( \frac{\tilde{\sigma}_j}{h_\nu} \right)^2 \right) f_j = 2 + C_2 \left( \frac{\sigma_i}{h_\nu} \right)^2 \quad (20)$$

In these equations,  $C_2$  is the second moment of vorticity along the x- or y-axis of a thick-cored particle whose radius is normalized by  $h_\nu$ , which for a true Gaussian is 0.5. Just as in the uniform-core-size method, if a solution to these equations does not exist, a new particle is placed in the vicinity of particle  $i$  with a post-step radius of  $\tilde{\sigma}_i$  and the procedure is repeated. Note that VRM allows solving to arbitrarily high moments [28], though the present work limits the solution to 2nd moments. Lakkis & Ghoniem [10] show increased error when VRM includes particles with core sizes different from the diffusing particle, so their method specifically excludes those other particles from the above calculation. But because particle core sizes in the present method are not quantized at all, and grow under a particle radius gradient constraint, neighboring particles have only slightly different radii, and any additional error is limited.

### Strength Thresholds

In the uniform-radius method, there must exist a threshold circulation ( $\varepsilon$ ) below which a particle will not shed circulation to its neighbors. This limits the infinite geometric growth of the particle distribution at the expense of accuracy at the edge of the vorticity support. We keep this threshold in our adaptive-radius method, but call it  $\varepsilon_{ignore}$ . We introduce another threshold,  $\varepsilon_{adapt}$ , which is the circulation magnitude above which the particle's core radius will not grow (it will diffuse via pure VRM). This leaves the range of circulations for which a particle will perform VRM and possibly grow to  $\varepsilon_{adapt} > |\Gamma| > \varepsilon_{ignore}$ . In the adaptive-radius method, if  $|\Gamma| < \varepsilon_{ignore}$ , the particle will not perform VRM, but will be allowed to grow only up to a specific size. This introduces some inaccuracies again at the edge of the vorticity support, but not as much as disallowing diffusion altogether.

### Selecting the Desired Radius

When solving the VRM equations, though, we must account for the different radii of the participating particles, and to do this correctly requires knowing the radii of all participating particles before and after the diffusion step. Two criteria will determine the desired particle sizes: the relative strength of the particle vs. a threshold, and a limitation on the spatial gradient of particle core sizes (called the *lapse ratio*). These criteria will determine how much of the particle's diffusion will be accounted for via a change in size (growth or shrinking) and via sharing its strength with its neighbors according to a solution to the VRM equations.

Our proposed spatially-adaptive VRM uses the following procedure:

1. Compute post-step core radii for all particles; for each particle whose strength magnitude is below the adaptivity threshold ( $\varepsilon_{adapt}$ ):
  - (a) Search nearby particles to find maximum size allowed by radius lapse ratio
  - (b) Determine new size if all diffusion goes into core-spreading
  - (c) Find minimum radius from these two calculations
  - (d) Set post-diffusion radius to be between this and the current radius
2. Perform VRM, using pre- and post-step radii to adjust the moment equations
3. Apply the strength and radius changes to all particles

The formulae for the desired new particle radius  $\tilde{\sigma}_i$ , given the radius lapse ratio  $C_{lapse}$  and second moment coefficient  $C_2$ , are as follows:

$$\sigma_{i,lapse} = \min \left[ \sigma_j + C_{lapse} \|\vec{x}_i - \vec{x}_j\|_2 \right]_{j \neq i} \quad (21)$$

$$\sigma_{i,grow} = \sqrt{\sigma_i^2 + 2 h_v^2 / C_2} \quad (22)$$

$$\sigma_{i,test} = \min \left[ \sigma_{i,lapse}, \sigma_{i,grow} \right] \quad (23)$$

$$\tilde{\sigma}_i = \begin{cases} \frac{3\sigma_i + \sigma_{i,test}}{4}, & \text{if } \sigma_{i,test} > \sigma_i \\ \max[\sigma_{i,test}, 0.9\sigma_i], & \text{if } \sigma_{i,test} < \sigma_i \end{cases} \quad (24)$$

Note that because of the averaging of the old and ideal radii the particles grow smoothly up to their desired radius, avoiding excessive grow-then-shrink cycles. Also, unlike Lakkis & Ghoniem [10], particle core sizes are not quantized and can take any value at or above the limit imposed by the global time step ( $\sigma_{min} = C_\sigma C_\delta \sqrt{v \Delta t}$ ). A final note is that the above method for determining particle core size is not exclusive of other methods—one can additionally allow particle sizes to increase linearly with distance from the origin or from a solid body, as is done frequently in the literature [10, 13, 15].

### Avoiding Excessive Overlap

Convective accuracy in LVPMs is hindered by velocity errors from excessive particle overlap [3] (and smoothness hindered by insufficient overlap), and in an incompressible flow with time-varying core radii, it is highly likely that particles will grow in size and overlap more with their neighbors. The solution for this is to merge neighboring particles while simultaneously conserving the moments of the local vorticity field [8]. In the present method, particles are allowed to merge if a measure of the relative error due the proposed merge is below a threshold; and when they merge, the 0th and 1st moments are conserved, and the new radius is set to minimize the error in the 2nd moment, in a manner similar to [4]. Note that the combined action of growth and merging serves to maintain approximately the same number of particles in each particles' radius-normalized neighborhood, a situation noted by Dehnen [9] as minimizing the error in “softened” (desingularized) N-body gravitational systems.

### Implementation

The open-source *Omega2D* [33] solver was used as the driver for the present method. This is an open-source, cross-platform, C++11/14/17 program with a graphical user interface, for performing LVPM simulations. All Biot-Savart summations in this program use direct  $O(N^2)$  summations, though algorithms with lower order of operations [34, 35] will be supported in the future. Nevertheless, extensive performance optimization using multi-threading and explicit vectorization [27] allow small simulations to run at interactive rates. All tests below were performed on a 16-core AMD Ryzen 9 3950X workstation running Fedora Linux.

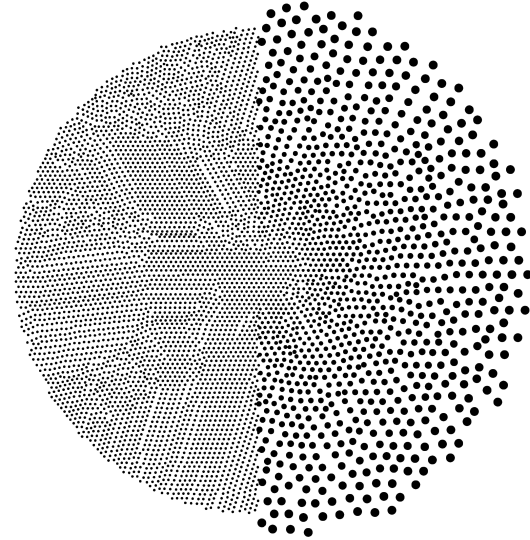


**FIGURE 1.** 2-D DIFFUSION PROBLEM, STEP 250, PARTICLE DISTRIBUTIONS, UNIFORM,  $N_V = 8,105$  (LEFT), ADAPTIVE,  $N_V = 2,458$  (RIGHT).

### VALIDATION

Two canonical flows were created and run with the present method: pure diffusion of a  $\delta$ -function and flow over an impulsively-started circular cylinder. In each case, the results indicate the method can significantly reduce the number of computational elements necessary to represent the system without an unreasonable loss of accuracy.

### Point Diffusion

The simplest test, diffusion of a  $\delta$ -function without convection, is an ideal test to compare uniform VRM with the proposed adaptive method. The resulting field at time  $t$  is the well-known Gaussian distribution.

$$\omega(r) = \frac{\Gamma}{4\pi v t} e^{-\frac{r^2}{4vt}} \quad (25)$$

The system is initialized with  $v = 1$  and a single particle of strength  $\Gamma = 1$ . Because the core function is a Gaussian with core radius  $\sigma = 2\sqrt{6v\Delta t}$ , the time is initialized to  $6\Delta t$  instead of 0 to account for diffusion of the  $\delta$ -function. Relative thresholds for VRM are  $\varepsilon_{ignore} = 10^{-6}$  and  $\varepsilon_{adapt} = 10^{-3}$ , and the adaptive case uses  $C_{lapse} = 0.1$ .

The above system was run with a variety of time step sizes  $\Delta t$ , each corresponding to a different particle core size. Errors in moment conservation were calculated for each run at  $t = 100$ , with even moments normalized by the theoretical value, and odd

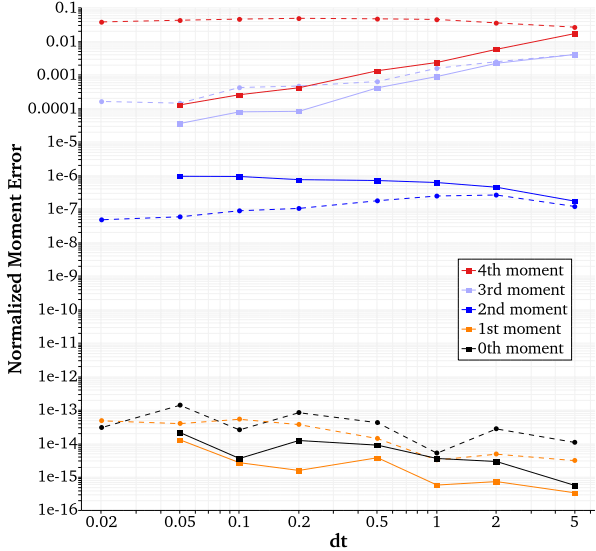


**FIGURE 2.** 2-D HEAT PROBLEM,  $\nu = 1$ ,  $T = 100$ , MOMENT CONSERVATION, UNIFORM (SOLID) AND ADAPTIVE (DASHED) CASES.

moments by the square root of the product of the adjacent (even) moments. Sample particle distributions (with point sizes scaled by particle radius) appear in Fig. 1 for the 250th time step of the  $\Delta t = 0.1$  case, where  $N_\nu = 8,105$  for the uniform run and  $N_\nu = 2,458$  for the adaptive run. Numerical results in Fig. 2 indicate that the 0th and 1st moments are resolved to approximately machine precision (double-precision is used for these calculations), while 2nd moment is conserved to approximately  $\varepsilon_{\text{ignore}}$ . Notable is that the adaptive case exhibits lower second moment errors than the uniform case—this is due to better resolution of the outer reaches of the field by particles with larger radii. Despite the VRM equations conserving up to only the second moment explicitly, the third moment for both uniform and adaptive runs decreases as resolution increases. Finally, the fourth moment for the adaptive case appears to suffer near-constant error while the uniform case shows a second-order convergence vs.  $h \sim \sqrt{\Delta t}$ .

Another test with  $\nu = 10^{-3}$  and  $\Delta t = 0.02$  illuminates the tradeoff between element count and pointwise error as a point diffuses. The error is measured using an  $L_2$  pointwise norm,  $h^2 \sqrt{\sum_i (\omega_i - \bar{\omega})^2}$ , integrated over 40,000 points in a regular lattice in the range  $\pm 8\sqrt{4\nu t}$  and compared to the true solution. Results for a uniform case and two adaptive cases, with  $C_{\text{lapse}} = 0.05$  and  $C_{\text{lapse}} = 0.1$ , appear in Fig. 3. The extra error associated with the adaptive scheme is clear here, but it comes with a substantial reduction in the number of particles necessary. With one-third as many particles, the  $L_2$  error doubles, while an 80% reduction in particles comes with a roughly 4-fold increase in error to  $3.4 \times 10^{-4}$ . Further progression of these test cases in time would

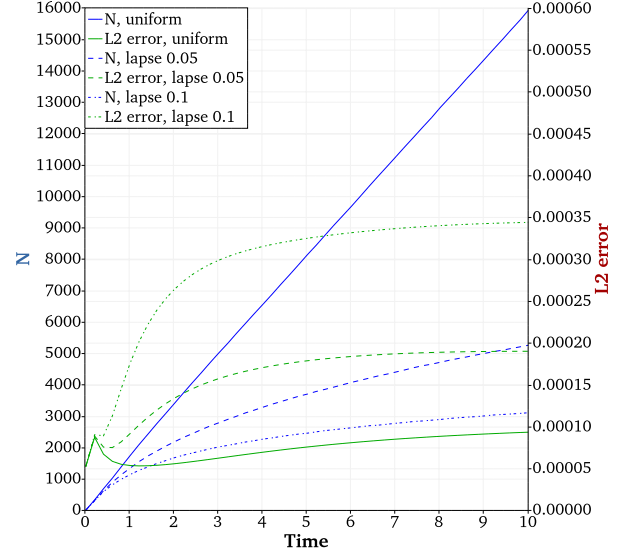


**FIGURE 3.** 2-D HEAT PROBLEM,  $\nu = 0.001$ ,  $\Delta T = 0.02$ , PARTICLE COUNT AND  $L_2$  INTEGRATED ERROR, UNIFORM (SOLID) AND ADAPTIVE (DASHED, DOTTED) CASES.

show improvement in the reduction of problem size with little extra loss of accuracy. Figure 15 in Lakkis & Ghoniem [10] shows that a case with two initial diffusing particles and variable-core variable-spacing with redistribution with variable cores (the most comparable to our method) achieves, after 500 steps,  $L_2$  error of 0.000365 with 7,500 particles (a single diffusing particle could be assumed to require a little more than 3,750). Our method with  $C_{\text{lapse}} = 0.1$  and larger  $\Delta t$ , after as many steps, demonstrates  $L_2$  error of 0.000345 while using 3,110 particles.

### Impulsively Started Cylinder at Re=9,500

Impulsively started flow over a circular cylinder is a well-studied problem in two-dimensional fluid dynamics. At intermediate Reynolds numbers, capturing the vorticity field correctly requires careful accounting of the vorticity creation at the boundary, something that has been a challenge for traditional LVPMs. Below we will demonstrate this canonical flow with  $Re_D = 9,500$ , study the influence of important parameters, and compare our results with previous computations [36–40].

This problem is frequently studied with LVPMs, most notably with Koumoutsakos & Leonard [36] using a PSE scheme for diffusion, Shankar [37] the same VRM as the present work, and Wang [39] a diffusion-velocity approach. In a recent implementation of the vortex penalization method [40], diffusion was accomplished with finite differences on a high-resolution regular grid. Our final comparison is with a spectral element method solution by Kruse [38], results of which were gathered from Shankar [37]. The studies by Lakkis & Ghoniem [10] and

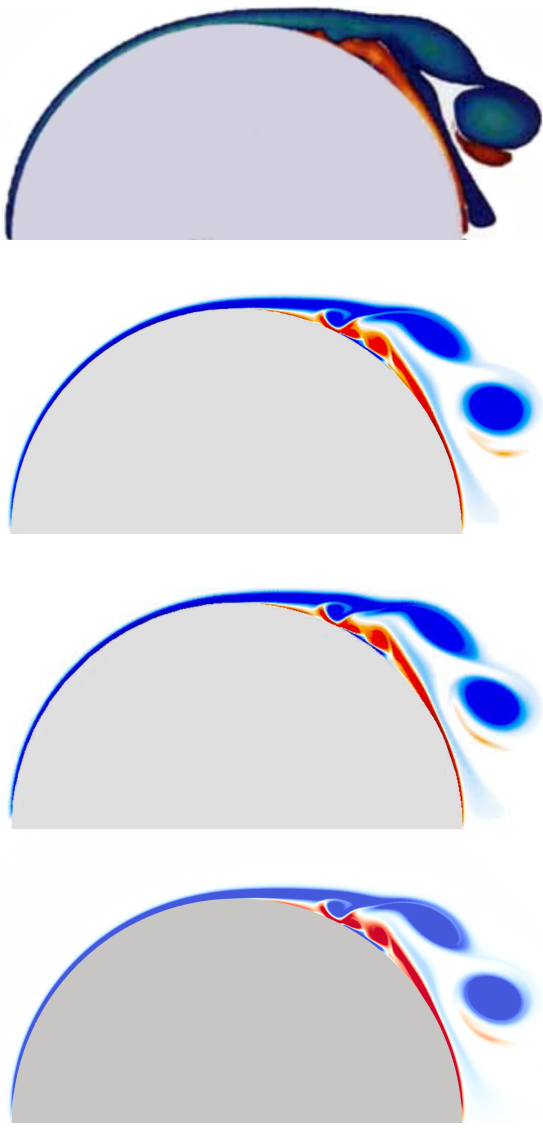


**FIGURE 4.** 2-D FLOW OVER IMPULSIVELY STARTED CYLINDER WITH  $Re_D = 9,500$ , VORTICITY FIELD AT  $T_R = 3$ , FROM REFERENCES [36], [38], [37], AND PRESENT METHOD (TOP TO BOTTOM).

Rasmussen *et al.* [19] exhibited results very similar to those of Shankar [37] and the present method. Other notable studies of this case [41, 42] did not present vorticity fields at the same time steps as the above.

The cases presented below use  $D = 1$ ,  $U_\infty = 1$ ,  $Re_D = 9,500$ , and were completed with our open-source *Omega2D* LVPM solver. The Biot-Savart integration uses the Vatistas  $n = 2$  compact core function [43], and the BEM uses constant-strength source

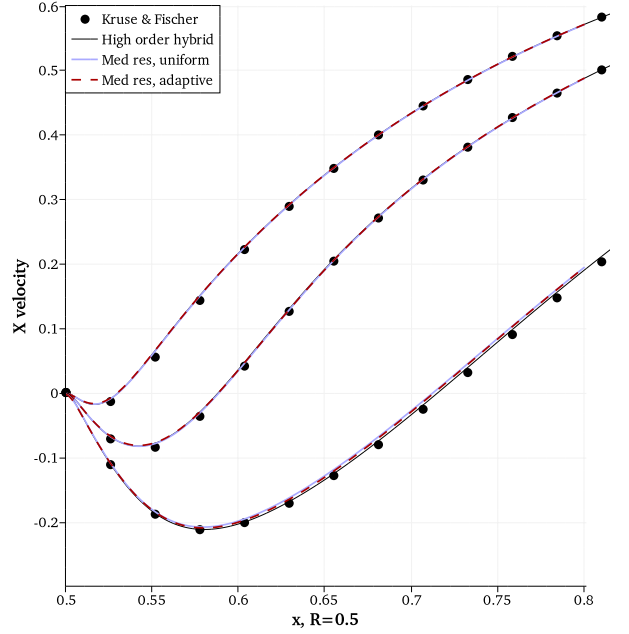


**FIGURE 5.** 2-D FLOW OVER IMPULSIVELY STARTED CYLINDER WITH  $Re_D = 9,500$ ,  $T_R = \{1,2,3\}$ , X-VELOCITY ALONG TRAILING CENTERLINE, FROM REFERENCES [38], [44], AND PRESENT METHOD WITH  $\Delta T_R = 0.01$ .

and vortex panels. Following previous authors, time reported in the figures is non-dimensionalized based on the cylinder radius, and most results will be reported at  $t_R = 3$  ( $t_D = 1.5$  if non-dimensionalized by diameter). Each vorticity field in the following figures is made by performing a Biot-Savart integration of the particles and panels onto an annular grid of  $80 \times 500$  2nd order quadrilateral elements in the range  $1 \leq r/R \leq 1.6$ . The simulation still proceeds in a Lagrangian manner—these Eulerian vorticity fields are for plotting only. With the exception of Figure 4, subsequent vorticity plots are made in ParaView with the “Cool to Warm (Extended)” palette and a range of  $\pm 80$ .

Figure 4 compares three previous methods to our results with  $\Delta t_R = 0.0025$ ,  $\varepsilon_{adapt} = 10^{-2}$ ,  $\varepsilon_{ignore} = 10^{-4}$ , and  $C_{lapse} = 0.15$ , which at  $t_R = 3$  required 240,662 particles. Details in the vorticity field downstream of the separation point are difficult to discern from the older references, but all four methods seem to capture the position and sizes of the secondary parcels of vorticity. The most notable difference is in the thin region of positive vorticity (red) immediately adjacent to the first primary shed vortex (blue), the magnitude of which is not reported in the literature, though the position is readily comparable. On this criterion, the present results more closely resemble the earlier VRM calculations than the spectral method. A second valuable comparison is the shape of the first primary vortex, which seems more circular in the

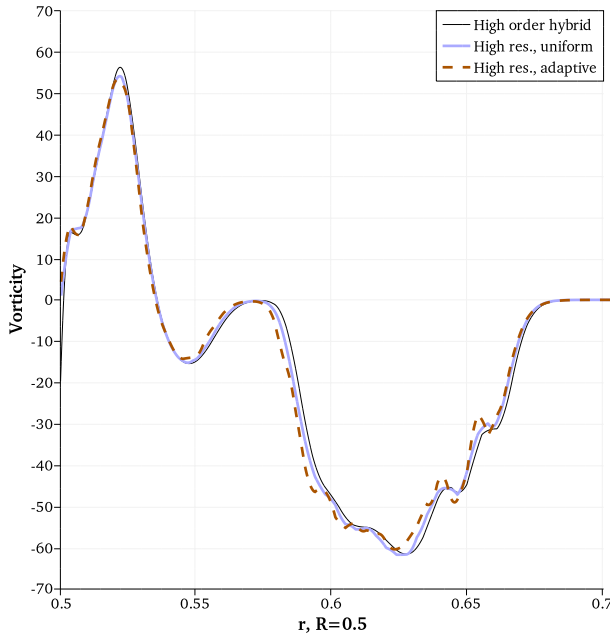


**FIGURE 6.** 2-D FLOW OVER IMPULSIVELY STARTED CYLINDER WITH  $RE_D = 9,500$ , VORTICITY ALONG  $45^\circ$  LINE AT  $t_R = 3$ , FROM REFERENCES [38], [44], AND PRESENT METHOD WITH  $\Delta t_R = 0.0025$ .

spectral results, but appears more oval-like in the others. The results of the adaptive-resolution VIC simulations of Rasmussen *et al.* [19] are very similar to the present method, though using a significantly smaller  $\Delta t_R = 10^{-4}$  and  $2.228 \times 10^6$  cells.

In Fig. 5 we investigate the streamwise velocity along a line emanating from the trailing stagnation node. Our medium resolution results ( $\Delta t_R = 0.01$ ) are compared with a high-order vorticity solver [44] and to the spectral method of Kruse [38]. Even though this plot is a close-up of the full set of data, the present method is imperceptibly different from the high-order solver, and strays only subtly from the spectral results.

Finally, we plot the vorticity at  $t_R = 3$  along a line emanating  $45^\circ$  from the trailing stagnation node, comparing our uniform and adaptive high-resolution results ( $\Delta t_R = 0.0025$ ) to the high-order vorticity-velocity results [44] in Fig. 6. This line was chosen because it slices through a complex part of the near-body region and also through the second, striated, positive vortex, revealing its inner structure. The high-order method adequately resolves the boundary layer, and shows negative vorticity immediately above the body, while the present Lagrangian method does not (the vorticity beneath the innermost layer of particles is in a bound vortex sheet whose strength is found using BEM). The high-order method also resolves the positive vorticity peak better than the two particle methods. Both particle methods capture the key parts of

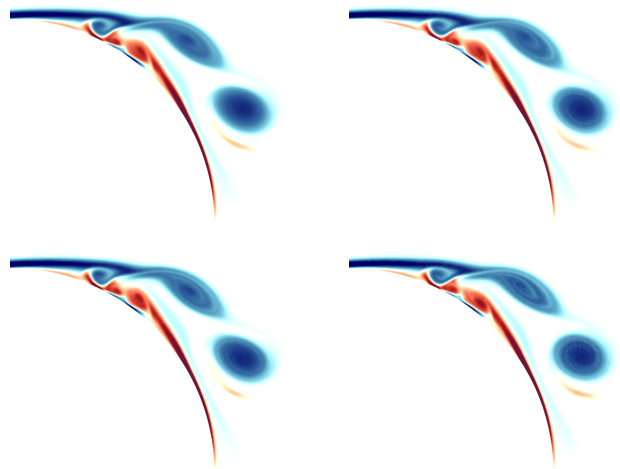


**FIGURE 7.** 2-D FLOW OVER IMPULSIVELY STARTED CYLINDER WITH  $RE_D = 9,500$ , VORTICITY FIELD AT  $t_R = 3$ ,  $\Delta t_R = 0.01$ , ADAPTIVITY THRESHOLDS  $\{\varepsilon_{ADAPT}, \varepsilon_{IGNORE}\}$  (TOP ROW):  $\{N.A., 10^{-5}\}$  (UNIFORM),  $\{10^{-3}, 10^{-6}\}$ , (BOTTOM ROW):  $\{10^{-2}, 10^{-4}\}$ ,  $\{10^{-1}, 10^{-2}\}$ .

**TABLE 1.** PARAMETERS AND RESULTS FOR IMPULSIVELY-STARTED CYLINDER SIMULATIONS, VARYING ADAPTIVITY THRESHOLDS.

Parameter	Uniform		Adaptive		
	$\varepsilon_{adapt}$	$\varepsilon_{ignore}$	$N_v$	$\Delta t_R$	Time to $t_R = 3$
$\varepsilon_{adapt}$	-	$10^{-3}$	$10^{-2}$	$10^{-1}$	
$\varepsilon_{ignore}$	$10^{-5}$	$10^{-6}$	$10^{-4}$	$10^{-2}$	
$N_v$	154,523	90,540	80,686	54,847	
Time to $t_R = 3$	16:29	11:20	9:57	7:19	

the structure of the outer vortex, but the adaptive scheme exhibits some overshoot in the weak laminae. Note that the high-order simulation required 98,280 third-order elements and over a day of computation, the uniform-core-size LVPM 598,073 particles and over six hours, and the adaptive method 239,901 and under three hours.

**Effect of adaptivity thresholds** To determine the influence of the adaptivity thresholds on the solution, three simulations with different thresholds were run and the results compared to the case with uniform particle size. Each simulation was run to  $t_R = 3$  using  $\Delta t_R = 0.01$  and a radius lapse rate of  $C_{lapse} = 0.15$ . Vorticity fields from these simulations appear in Fig. 7 and the corresponding parameters (where they vary) in Table 1. While subtle differences exist between the four cases, all appear to cap-

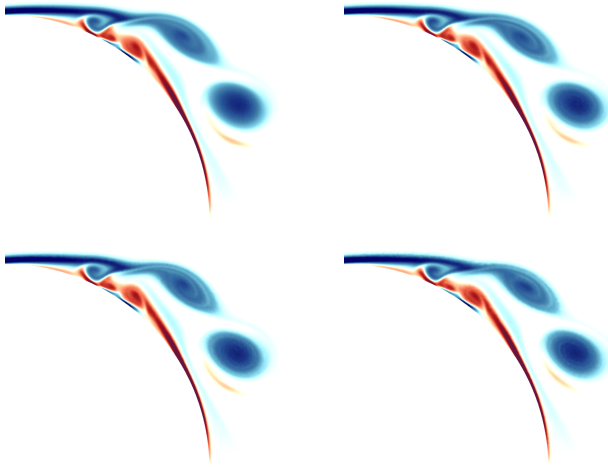


**FIGURE 8.** 2-D FLOW OVER IMPULSIVELY STARTED CYLINDER WITH  $Re_D = 9,500$ , VORTICITY FIELD AT  $t_R = 3$ ,  $\Delta t_R = 0.01$ , RADIUS LAPSE RATES (TOP ROW): 0 (UNIFORM), 0.1, (BOTTOM ROW): 0.2, 0.4.

**TABLE 2.** PARAMETERS AND RESULTS FOR IMPULSIVELY-STARTED CYLINDER SIMULATIONS, VARYING LAPSE RATES.

Parameter	Uniform	Adaptive		
$C_{lapse}$	0	0.1	0.2	0.4
$N_v$	154,523	87,049	77,469	74,637
Time to $t_R = 3$	16:29	10:43	9:43	9:26

ture the oval-shaped primary vortex (blue), the striated secondary coalescing vortex (blue), and the arrangement and size of the small number of wall-bounded vortices. A noticeable difference is the shape of the primary vortex, with the most aggressive level of adaptivity ( $\varepsilon_{adapt} = 10^{-1}$ ) resulting in a more circular vortex with noticeable striations. The performance data reveal that, even at this early stage, the particle count and wall-clock time can be cut in half with little effect on the vorticity.

**Effect of radius lapse rate** Recall that the radius lapse rate  $C_{lapse}$  is the maximum allowable change in particle radius per unit distance between particles. Enforcing this puts a limit on the range of particle radii that participate in any VRM solution. Tests were run with  $\Delta t_R = 0.01$ , relative thresholds  $\varepsilon_{ignore} = 10^{-4}$  and  $\varepsilon_{adapt} = 10^{-2}$ , and varying  $C_{lapse}$  from 0 (uniform) to 0.4 (very aggressive). Vorticity fields for these simulations appear in Fig. 8. One subtle but noticeable difference involves the position of the thin wisp of positive vorticity (red) just below

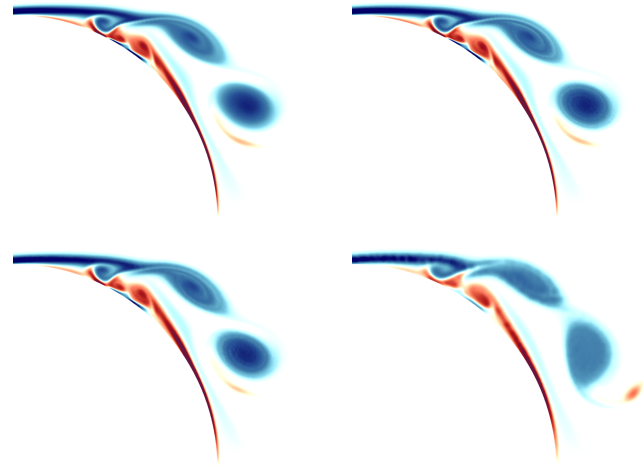


**FIGURE 9.** 2-D FLOW OVER IMPULSIVELY STARTED CYLINDER WITH  $Re_D = 9,500$ , VORTICITY FIELD AT  $t_R = 3$ , VARYING PARTICLE RESOLUTIONS (TOP ROW):  $\Delta t_R = 0.0025$  UNIFORM AND ADAPTIVE, (BOTTOM ROW):  $\Delta t_R = \{0.01, 0.04\}$  ADAPTIVE.

**TABLE 3.** PARAMETERS AND RESULTS FOR IMPULSIVELY-STARTED CYLINDER SIMULATIONS, VARYING PARTICLE RESOLUTION.

Parameter	Low	Medium	High
$\Delta t_R$	0.04	0.01	0.0025
$\Delta x$	0.003554	0.001777	0.000889
$N_v$ uniform	40,611	154,523	598,073
$N_v$ adaptive	26,502	80,686	239,901
Time to $t_R = 3$ , unif.	0:51.3	16:29	6:43:58
Time to $t_R = 3$ , adapt.	0:39.4	9:57	2:39:54

the first primary negative vortex (blue), which is smaller and further rotated around the primary vortex when  $C_{lapse} = 0.4$ , more similar to the Shankar [37] results from Fig. 4, than of present results with higher resolution. In addition, the  $C_{lapse} = 0.4$  case exhibits a smaller wall-bounded positive vortex (red) than the other cases. Numerical results in Table 2 show little difference between the  $C_{lapse} = 0.2$  and 0.4 cases, though that is unlikely to be the case for longer runs with more diffused wakes.

**Effect of particle resolution** We finally examine the effect of particle resolution on the results. Because interparticle spacing varies with time step size as  $\Delta x = \sqrt{6v\Delta t_D}$ , smaller time steps require more particles and longer run time. Param-

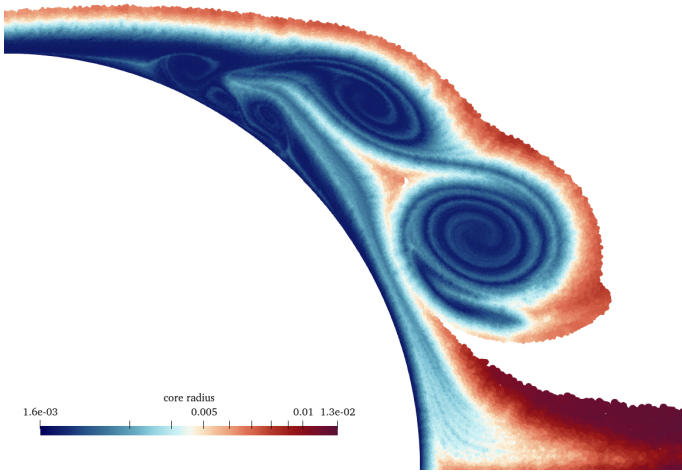


**FIGURE 10.** 2-D FLOW OVER IMPULSIVELY STARTED CYLINDER WITH  $RE_D = 9,500$ , DISTRIBUTION OF PARTICLE CORE RADII AT  $T_R = 3$ ,  $\Delta T_R = 0.0025$ .

ters common to adaptive runs are  $\varepsilon_{ignore} = 10^{-4}$ ,  $\varepsilon_{adapt} = 10^{-2}$ , and  $C_{lapse} = 0.15$ , while the uniform resolution runs used  $\varepsilon_{ignore} = 10^{-5}$ . Table 3 presents the varying parameters and quantitative results, while vorticity fields at  $t_R = 3$  for select runs appear in Fig. 9. Readily apparent is the unconvolved low-resolution result—the primary vortex is misshapen and its orbiting red vortex patch is not elongated like the other results. As particle resolution increases, though, the adaptive results quickly approach the uniform high resolution case. By way of comparison, Lakkis & Ghoniem [10] achieve similarly good results with their adaptive method using 200,000 particles with  $\Delta t_R = 0.01$ .

Figure 10 illustrates clearly that the present method adapts the particle core sizes to the solution, as demanded by the adaptivity thresholds and the radius lapse rate. More and smaller particles are used to resolve the vortices and boundary layer, and fewer, larger particles the outer reaches of the vorticity.

## CONCLUSIONS

A fully-local and solution-adaptive spatial adaptivity scheme for Lagrangian Vortex Particle Methods requiring no *a priori* knowledge of regions of interest and no regridding or remeshing of any kind has been devised and tested. It effectively maintains resolution near boundaries and in areas of high vorticity, while reducing particle density in areas of lesser importance. The performance benefits increase as resolution and simulation length increase and the concept is extensible to three dimensions with little extra effort.

## ACKNOWLEDGMENT

Research reported in this publication was supported by the National Institute Of Biomedical Imaging And Bioengineering of the National Institutes of Health under Award Number R01EB022180. The content is solely the responsibility of the authors and does not necessarily represent the official views of the National Institutes of Health.

## REFERENCES

- [1] Chorin, A. J., 1973. “Numerical study of slightly viscous flow”. *J. Fluid Mech.*, **57**, pp. 785–796.
- [2] Kuwahara, K., and Takami, H., 1973. “Numerical studies of two-dimensional vortex motion by a system of point vortices”. *J. Phys. Soc. Japan*, **34**(1), pp. 247–253.
- [3] Greengard, L., 1985. “The core spreading vortex method approximates the wrong equation”. *J. Comput. Phys.*, **61**, pp. 345–348.
- [4] Rossi, L. F., 1996. “Resurrecting core spreading vortex methods: A new scheme that is both deterministic and convergent”. *SIAM J. Sci. Comput.*, **17**(3), pp. 370–397.
- [5] Mas-Gallic, S., 1987. “Contribution à l’analyse numérique des méthodes particulières”. PhD thesis, Université Paris VI.
- [6] Degond, P., and Mas-Gallic, S., 1989. “The weighted particle method for convection-diffusion equations, Part 1: The case of an isotropic viscosity”. *Math. Comput.*, **53**(188), pp. 485–507.
- [7] Shankar, S., and van Dommelen, L., 1996. “A New Diffusion Procedure for Vortex Methods”. *J. Comput. Phys.*, **127**, pp. 88–109.
- [8] Spalart, P. R., 1988. “Vortex Methods for Separated Flows”. Tech. Rep. NASA TM-100068.
- [9] Dehnen, W., 2001. “Towards optimal softening in three-dimensional N-body codes - I. Minimizing the force error”. *Mon. Not. R. Astron. Soc.*, **324**, pp. 273–291.
- [10] Lakkis, I., and Ghoniem, A., 2009. “A high resolution spatially adaptive vortex method for separating flows. Part I: Two-dimensional domains”. *J. Comput. Phys.*, **228**(2), pp. 491–515.
- [11] Beale, J. T., and Majda, A., 1982. “Vortex methods I: Convergence in three dimensions”. *Math. Comput.*, **29**(159), pp. 1–27.
- [12] Hou, T. Y., Lowengrub, J., and Shelley, M. J., 1991. “Exact desingularization and local regridding for vortex methods”. *Lectures in Applied Mathematics: Vortex Methods and Vortex Dynamics*, pp. 341–362.
- [13] Salihi, M. L. O., 1998. “Couplage de méthodes numériques en simulation directe d’écoulements incompressibles”. PhD thesis, Université Joseph-Fourier-Grenoble I.
- [14] Cottet, G.-H., Koumoutsakos, P., and Salihi, M. L. O., 2000.

- “Vortex methods with spatially varying cores”. *J. Comput. Phys.*, **162**(1), pp. 164–185.
- [15] Ploumhans, P., Winckelmans, G. S., Salmon, J. K., Leonard, A., and Warren, M. S., 2002. “Vortex methods for direct numerical simulation of three-dimensional bluff body flows: Application to the sphere at  $Re=300, 500,$  and  $1000$ ”. *J. Comput. Phys.*, **178**, pp. 427–463.
- [16] Barba, L., Leonard, A., and Allen, C., 2005. “Advances in viscous vortex methods—meshless spatial adaption based on radial basis function interpolation”. *Intl. J. Numer. Methods Fluids*, **47**(5), pp. 387–421.
- [17] Reboux, S., Schrader, B., and Sbalzarini, I. F., 2012. “A self-organizing lagrangian particle method for adaptive-resolution advection–diffusion simulations”. *J. Comput. Phys.*, **231**(9), pp. 3623–3646.
- [18] Bergdorf, M., Cottet, G.-H., and Koumoutsakos, P., 2005. “Multilevel adaptive particle methods for convection–diffusion equations”. *Multiscale Modeling & Simulation*, **4**(1), pp. 328–357.
- [19] Rasmussen, J. T., Cottet, G.-H., and Walther, J. H., 2011. “A multiresolution remeshed vortex-in-cell algorithm using patches”. *J. Comput. Phys.*, **230**(17), pp. 6742–6755.
- [20] Teng, Z.-H., 1982. “Elliptic-vortex method for incompressible flow at high reynolds number”. *J. Comput. Phys.*, **46**(1), pp. 54–68.
- [21] Rossi, L. F., 2006. “A comparative study of Lagrangian methods using axisymmetric and deforming blobs”. *SIAM J. Sci. Comput.*, **27**(4), pp. 1168–1180.
- [22] Rossi, L. F., 2006. “Evaluation of the biot–savart integral for deformable elliptical gaussian vortex elements”. *SIAM J. Sci. Comput.*, **28**(4), pp. 1509–1532.
- [23] Häckli, C., Reboux, S., and Sbalzarini, I. F., 2015. “A self-organizing adaptive-resolution particle method with anisotropic kernels”. *Procedia IUTAM*, **18**, pp. 40–55.
- [24] Cottet, G.-H., and Koumoutsakos, P., 1999. *Vortex Methods: Theory and Practice*. Cambridge Univ. Press, Cambridge, UK.
- [25] Gharakhani, A., 2007. “3-D Vortex Simulation Of Accelerating Flow Over A Simplified Opening Bileaflet Valve”. In Proceedings of FEDSM2007 5th Joint ASME/JSME Fluids Engineering Conference, no. FEDSM2007-37134.
- [26] Stock, M. J., and Gharakhani, A., 2011. “Graphics Processing Unit-Accelerated Boundary Element Method and Vortex Particle Method”. *J. Aero. Comp. Inf. Com.*, **8**(7), July, pp. 224–236.
- [27] Stock, M. J., and Gharakhani, A., 2020. “Open-source accelerated vortex particle methods for unsteady flow simulation”. In Proceedings of the ASME 2020 Fluids Engineering Division Summer Meeting, Vol. FEDSM2020-83730.
- [28] Gharakhani, A., 2000. “A higher order vorticity redistribution method for 3-D diffusion in free space”. Tech. Rep. Report No. SAND2000-2505, Sandia National Laborato-
- ries.
- [29] Schrader, B., Reboux, S., and Sbalzarini, I. F., 2010. “Discretization correction of general integral pse operators for particle methods”. *J. Comput. Phys.*, **229**(11), pp. 4159–4182.
- [30] Guennebaud, G., Jacob, B., et al., 2010. “Eigen v3”. <http://eigen.tuxfamily.org>.
- [31] Abdelmalek, N. N., 1977. “Minimum  $L_\infty$  Solution of under-determined systems of linear equations”. *J. Approx. Theory*, **20**, pp. 57–69.
- [32] Lakkis, I., and Ghoniem, A. F., 2003. “Axisymmetric vortex method for low-mach number, diffusion-controlled combustion”. *J. Comput. Phys.*, **184**(2), pp. 435–475.
- [33] Stock, M. J., and Gharakhani, A., 2020. “Omega2D: Two-Dimensional Flow Solver with GUI Using Vortex Particle and Boundary Element Methods”. <https://github.com/Applied-Scientific-Research/Omega2D>.
- [34] Barnes, J. E., and Hut, P., 1986. “A Hierarchical  $O(N \log N)$  Force Calculation Algorithm”. *Nature*, **324**, pp. 446–449.
- [35] Greengard, L., and Rokhlin, V., 1987. “A Fast Algorithm for Particle Simulations”. *J. Comput. Phys.*, **73**, pp. 325–348.
- [36] Koumoutsakos, P., and Leonard, A., 1995. “High-resolution simulations of the flow around an impulsively started cylinder using vortex methods”. *J. Fluid Mech.*, **296**, pp. 1–357.
- [37] Subramaniam, S., 1996. “A new mesh-free vortex method”. PhD thesis, Florida State University.
- [38] Kruse, G. W., 1997. “Parallel nonconforming spectral element methods”. PhD thesis, Brown University.
- [39] Wang, L., 2016. “High-performance discrete-vortex algorithms for unsteady viscous-fluid flows near moving boundaries”. PhD thesis, University of California, Berkeley.
- [40] Lee, S.-J., 2017. “Numerical simulation of vortex-Dominated flows using the penalized VIC method”. In *Vortex Dynamics and Optical Vortices*, InTech, pp. 55–83.
- [41] Chang, C.-C., and Chern, R.-L., 1991. “Vortex Shedding From an Impulsively Started Rotating and Translating Circular Cylinder”. *J. Fluid Mech.*, **233**, pp. 265–298.
- [42] Rossinelli, D., Hejazialhosseini, B., van Rees, W., Gazzola, M., Bergdorf, M., and Koumoutsakos, P., 2015. “MRAG-I2D: Multi-resolution adapted grids for remeshed vortex methods on multicore architectures”. *J. Comput. Phys.*, **288**, pp. 1–18.
- [43] Vatistas, G. H., Kozel, V., and Mih, W., 1991. “A simpler model for concentrated vortices”. *Exp. Fluids*, **11**(1), pp. 73–76.
- [44] Stock, M., and Gharakhani, A., 2021. “A Hybrid High-Order Vorticity-Based Eulerian and Lagrangian Vortex Particle Method, the 2-D Case”. In Proceedings of the ASME 2021 Fluids Engineering Division Summer Meeting, no. FEDSM2021-65637.